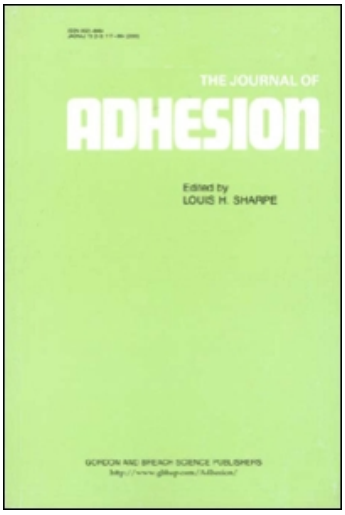

The Journal of Adhesion
Publication details, including instructions for authors and subscription information:
http://www.informaworld.com/smpp/title~content=t713453635

Molecular Dynamic Modeling of Particle Adhesion

D. J. Quesnel[ab]; D. S. Rimai[ab]; L. P. Demejo[ab]
[a] Mechanical Engineering Department, University of Rochester, Rochester, NY, USA [b] Office Imaging Research and Technology Development, Eastman Kodak Company, Rochester, NY, USA

To cite this Article Quesnel, D. J. , Rimai, D. S. and Demejo, L. P.(1995) 'Molecular Dynamic Modeling of Particle Adhesion', The Journal of Adhesion, 51: 1, 49 — 69
To link to this Article: DOI: 10.1080/00218469508009989
URL: http://dx.doi.org/10.1080/00218469508009989

J. Adhesion, 1995, Vol. 51, pp. 49–69
Reprints available directly from the publisher
Photocopying permitted by license only

Molecular Dynamic Modeling of Particle Adhesion*

D. J. QUESNEL, D. S. RIMAI and L. P. DEMEJO

Mechanical Engineering Department, University of Rochester, Rochester NY 14627-0132, USA
Office Imaging Research and Technology Development, Eastman Kodak Company, Rochester NY 14653-6402, USA

(Received June 27, 1994; in final form December 16, 1994)

Molecular dynamic modeling was used to study the interactions between nanometer size two-dimensional particles in proximity to the surface of a two-dimensional crystal composed of the same material. The modeling was conducted by using triangular lattices of atoms that interact through a Lennard-Jones potential. The atoms were configured such that the particle consisted of a circle with 463 atoms. The crystal was in the shape of a rectangle and contained 442 atoms. The system was assumed to have periodic boundary conditions. It was first allowed to equilibrate with an assumed dimensionless kinetic energy per atom of $0.2\,\varepsilon$. Subsequently, the particle was made to approach the surface at a velocity of $0.387\,\sigma/t$ (corresponding to 6.25 m/s for argon), which is small compared with the speed of sound in the material. The approach was conducted in two modes: (1) centroidal displacement control at constant temperature and (2) free flight at the same intercentroidal velocity of approach. For each case, the intercentroidal distance, velocity, and forces were determined as the particle approached, made contact, and relaxed into the surface. The computation followed the response of the system for a total of 11900 iterations (corresponding to 2.54 ns for argon). The particles and surfaces were found to deform before, during and after impact. Surface forces were sufficiently large to prevent the particles from separating from the substrate following the collision. The excess energy generated acoustic waves and lattice defects. The geometry of the system at selected times was used to illustrate the deformations that occur. Results based on a molecular statics approach are also presented for comparison with analytical models based on potentials. Finally, preliminary results of a particle being removed from the substrate are presented.

KEY WORDS particle adhesion; Lennard-Jones potential; molecular dynamic modeling; deformation; adhesion hysteresis; impact velocity; particles approaching surfaces.

INTRODUCTION

The problem of the interaction between particles and substrates is of substantial interest to the scientific and engineering communities. This interest focuses on the desire to understand the mechanisms causing particles to adhere to surfaces. Such understanding should lead to greater control over our ability to place and remove particles from surfaces in ways that are technologically beneficial.

The mechanics of particle adhesion and the deformations resulting from the stresses generated by the forces of adhesion have been studied both theoretically and experimentally for many years and continue to be of interest. Reviews of recent

* Presented at the Seventeenth Annual Meeting of The Adhesion Society, Inc., in Orlando, Florida, U.S.A., February 21–23, 1994.

experimental developments have been presented elsewhere[1,2] and are beyond the scope of this paper. This paper will summarize key theoretical developments and report novel results obtained using molecular dynamic modeling.

Adhesion-induced deformations were first postulated, independently, by Bradley[3,4] and Derjaguin.[5] Derjaguin attempted to calculate the contact radius resulting from the adhesion forces by assuming that the particles acted as Hertzian indentors with the applied load, P°, arising exclusively from van der Walls interactions. Accordingly, he found that the contact radius, a, for a rigid particle in contact with a compliant substrate, would be related to the particle radius, R, by

$$a^3 = 3/4\, P^\circ \left[\frac{(1-\nu^2)}{E}\right] R \tag{1}$$

where ν and E are the Poisson's ratio and Young's modulus, respectively, of the substrate and P° is given by

$$P^\circ = \frac{\hbar\bar{\omega}}{8\pi z_0^2} R \tag{2}$$

where z_0 is the separation distance between the particle and substrate (typically about 4 Å) and $\hbar\bar{\omega}$ is the Hamaker coefficient.

Krupp[6] attempted to generalize Derjaguin's model of particle adhesion to allow for cases where the stress exceeded the yield strength of the material. He assumed that the contact area could be divided into two concentric regions: an inner region of radius a_1 which, being subjected to higher stresses, would deform plastically and an outer annulus extending from radius, a_1, to the total contact radius, a_0, which, being subjected to lower stresses, would deform elastically. Accordingly,

$$\pi a_0^2 = \frac{P^\circ}{H(t)} + \frac{1}{3}\left[\frac{\pi^{3/2}(1-\nu^2)RH(t)}{2E}\right]^2 \tag{3}$$

and

$$\pi a_1^2 = \frac{P^\circ}{H(t)} + \frac{1}{3}\left[\frac{\pi^{3/2}(1-\nu^2)RH(t)}{2E}\right]^2 \tag{4}$$

where $H(t)$ is a phenomenologically-determined, time-dependent hardness. In order to allow the contact radius to reach a limiting size, Krupp assumed that $H(t)$ approached an asymptotic value of the order of $10^{-3}\,E$ within approximately 30 minutes.

The classical theories of particle adhesion, which were just discussed, assumed that all interactions were compressive. Modern understanding, which began with the theory by Johnson *et al.* (hereafter referred to as JKR), recognized that both compressive and tensile interactions can occur. According to the JKR theory, all interactions occur within the contact zone and the resulting deformations are elastic. Approaching the problem from a thermodynamic rather than molecular viewpoint, the JKR model predicts that the contact radius is related to the particle radius by

$$a^3 = \frac{R}{K}\{P + 3w_A\pi R + [6w_A\pi RP + (3w_A\pi R)^2]^{1/2}\} \tag{5}$$

where P is any externally applied load, w_A is the work of adhesion and is related to the surface energies γ_1 and γ_2 and the interfacial energy γ_{12} by

$$w_A = \gamma_1 + \gamma_2 - \gamma_{12} \tag{6}$$

and

$$K = \frac{4}{3\pi(k_1 + k_2)} \tag{7}$$

where

$$k_i = \frac{1 - \nu_i^2}{\pi E} \tag{8}$$

and i assumes the values of 1 or 2 for the two materials involved. According to the JKR theory, upon application of a negative load, separation of the particle from the substrate would occur when an external force, P_s, was applied such that

$$P_s = -\frac{3}{2} w_A \pi R \tag{9}$$

Moreover, the contact radius at separation does not vanish but, rather, is approximately 63% of the contact radius obtained with no applied load. It is interesting to note that P_s does not depend on the Young's moduli of the materials and does not account for hysteretic effects. Although Johnson *et al.* were aware that hysteretic effects occur, particularly in polymers, they assumed that they were due to non-equilibrium conditions existing under separation conditions. As will be shown later in this paper, such hysteresis is a natural result of adhesion even for the case of elastic deformations.

Derjaguin[8] *et al.* proposed an alternative adhesion model (hereafter referred to as the DMT model), which also allowed for tensile interactions, but approached the problem form a molecular level. According to the DMT theory, the shape of the contact region continues to be Hertzian, as it was in the earlier model by Derjaguin. This assumption results in the prediction that half of the interactions occur outside the contact region, which is in contrast to a fundamental assumption of the JKR model.

The assumptions and predictions of the JKR and DMT models were compared by Tabor,[9] who showed that the DMT model predicts contact radii and separation forces of approximately 1/2 and 4/3, respectively, of those predicted by the JKR theory. Following some debate in the literature concerning these discrepancies,[10,11] Muller *et al.* proposed the MYD model.[12,13] In this model it is assumed that the adhesion forces between a particle and a substrate can be described by a pair-wise summation between the molecules of the two materials interacting *via* a Lennard-Jones potential. Muller *et al.* found that the both the JKR and DMT models were special cases of this more general theory, with the JKR model being valid for low modulus, high surface energy materials and larger particles, whereas the DMT model was valid for more rigid materials having lower surface energies and for smaller particles. The transition between the JKR and DMT models has recently been investigated by Maugis.[14,15] Others studying the contact region between particles and surfaces include Tsai *et al.*,[16] Dahneke,[17] Attard and Parker,[18,19] and Maugis and Pollock.[20]

Rogers and Reed[21] have explored the effect of particle-substrate impacts, resulting in plastic and elastic deformations, on adhesion. This area was further investigated by Reed[22] and by Wall *et al.*[23] In these models it is assumed that the only energy loss mechanism occurs through the plastic, not the elastic, deformations. More recently Johnson and Pollock[24] explored the effect on adhesion of a particle impacting a surface, using the JKR model.

The aforementioned theories have been instrumental in advancing current understanding of particle adhesion. However, all treat the mechanical response of the materials as factors that are totally independent of the parameters which affect adhesion. In reality, the intermolecular potential of a material determines both the mechanical properties and surface energy. It should, at least in theory, be possible to construct an adhesion model in a more holistic manner from first principles. Also, recent experimental advances have shown that the process of particle adhesion is more complicated than previously assumed. For example, as has been shown by Mizes *et al.*[25] and by Schaefer *et al.*[26,27] using atomic force techniques, the process of a particle impinging onto a surface becomes complex when the particle is in close proximity to that surface. At that time the attractive potential is sufficiently great as to cause the particle to jump into contact with the substrate, with the resulting energy being dissipated in the two materials. In addition, current theories do not always predict the correct power law dependence of the contact radius on particle radius. For example, it has been found that the contact radius of micrometer size particles in contact with elastomeric substrates can vary as the particle radius to the 3/4 power[28-30] rather than to the 2/3 power, as predicted by the JKR theory.

This paper reports results obtained from a first principle approach to the problem of particle adhesion. As such, it is part of a continuing series of papers in which the mechanical and adhesional properties of materials are determined. In addition, the interactions between surfaces and energy loss mechanisms in the presence of elastic deformations are studied. In two previous manuscripts[31,32] the Poisson's ratio and elastic constants were determined for an FCC lattice interacting *via* a Lennard-Jones potential. The interfacial energy between two surfaces was reported in a third paper.[33] In this paper the techniques developed previously have been expanded to model the interactions between a two-dimensional particle and a two-dimensional surface.

THE MODEL

As previously discussed, this work builds on earlier studies wherein it was assumed that particles interact *via* a Lennard-Jones potential, ϕ, given by

$$\phi = -4\varepsilon\left[\left(\frac{\sigma}{r}\right)^6 - \left(\frac{\sigma}{r}\right)^{12}\right] \tag{10}$$

where ε is the binding energy between one atom and its nearest neighbor and σ represents the spacing between atoms when the potential crosses the axis. It is recognized that the choice of this potential is idealistic. However, much understanding of the interactions

between particles and substrates can be readily obtained, at least qualitatively, using an idealized potential. Moreover, the use of such a relatively simple potential makes this and similar calculations practical on work stations, rather than requiring supercomputers. However, simply substituting the appropriate potential into the code and running it on a more powerful machine results in more quantitative predictions. Similarly, larger systems can also be modeled using larger computers.

Details of the model and computational techniques have been presented elsewhere.[32] They are presently summarized for the benefit of the reader. Additions to the model that tailor it to the problem of adhesional interactions between particles and substrates are also discussed.

In this work the stress-strain relationships and interfacial energy calculations for solids reported previously[31-33] are used to describe the interactions between a particle and a substrate. In the present calculations, both the particle and the substrate were treated as collections of discrete atoms of the same material interacting by the Lennard-Jones potential. The two bodies were first brought together and later separated under controlled conditions. Particular attention was paid to the forces, velocities, and displacements. Detailed atomic rearrangements are reported as "pictures" of the structure at specific times during the computational runs. The initial computations reported here were performed in two dimensions to gain insight into the three-dimensional contact between a sphere and a plane. This geometry, however, can also be considered a direct representation of the line contact between a cylinder and a plane.

The code used in the present calculations is an expressly revised version of a three-dimensional computer code, written by the authors, for desktop workstations.[32,33] It is part of a SMALL SCALE MOLECULAR DYNAMICS effort enabling scientists and engineers to perform useful computations on relatively powerful workstations that are currently available in the workplace. While specialized research tools and techniques exist to model very large systems directly with an eye towards quantitative predictions, much of the essential physics can be captured using the methods discussed in this paper.

The computations reported here were run on a SUN 4 workstation operating at about 15 Mflop/s. For this code, 10,000 iterations with 905 atoms require approximately 24 hours of dedicated CPU time.

The code is based on implementation of Verlet's algorithm[34,35] using three arrays of position co-ordinates to represent the past, present, and future atomic positions. Periodic boundary conditions were employed in a floating reference frame, which allowed the system to move in space. Look-up tables were used for the potentials to improve computational speed. In order to save time in computing the forces on each atom, lists of neighbors were used and updated during the process of deformation and during relative particle/surface motion. Stress and strain tensors were calculated during each iteration. The temperature and pressure were controlled by feedback loops that caused each computed value of T and P to approach a setpoint value by minimizing the error, like a laboratory controller.

All computations were performed using dimensionless units. Each iteration corresponds to 0.01 dimensionless time units. For the case of argon, which is the archetypical Lennard-Jones material, the fundamental units take on the following physical values.[31,32]

distance: $\sigma = 3.440 \times 10^{-10}$ meter
energy: $\varepsilon = 1.725 \times 10^{-21}$ joule/atom
mass: $m = 6.624 \times 10^{-26}$ kilogram/atom

Other derived units have the following physical values for argon:

time	t	$= \sigma(m/\varepsilon)^{1/2} = 2.132 \times 10^{-12}$ s
velocity:	σ/t	$= \sqrt{\varepsilon/m} = 1.614 \times 10^{2}$ m/s
acceleration:	σ/t^2	$= 7.568 \times 10^{13}$ m/s^2
stress:	ε/σ^3	$= 42.38 \times 10^{6}$ N/m^2
force:	ε/σ	$= 5.015 \times 10^{-12}$ N
stiffness:	ε/σ^2	$= 1.458 \times 10^{-2}$ N/m

Temperature may be interpreted as 2/3 of the mean kinetic energy expressed in ε units where

$$\begin{aligned}\varepsilon &= (125\,\text{K}) \cdot k \\ &= (125\,\text{K})(1.38 \times 10^{-23}\,\text{joule/atom/K}) \\ &= 1.725 \times 10^{-21}\,\text{J/atom}\end{aligned}$$

The computations were started by placing the atoms on their lattice sites with velocities selected using a Maxwell-Boltzmann distribution. The initial temperature of the system was set to approximately twice (2.6 times in two dimensions) the average kinetic energy. This way, once the kinetic energy equi-partitioned with the potential energy, the temperature would be approximately the value desired.

A two-dimensional triangular lattice comprised of a two-dimensional, face-centered rectangular unit cell was employed. The lattice of the particle (circle) was rotated 30° with respect to the lattice of the surface (rectangle), which was oriented with the rectangular unit cell parallel to the free surface. This rotation was performed to avoid any "instant coherency" between the particle and the surface, upon approach.

The periodic boundary conditions in the Z-direction were set to 100σ. This effectively allowed the three-dimensional code to function in only two dimensions. Periodic boundaries in the Y-direction were chosen so that one cutoff radius existed between the circle and the free surfaces of the rectangle. Thus, the circle and rectangle were, initially, non-interacting. In the X-direction, the periodic boundaries were set to an integral number of interatomic spacings for the lattice of interest so that normal stresses in the X-direction would be small. Thus it is clear that, while spatially periodic boundaries were used, the combination of these boundaries with finite cut-off radii and open spaces allows non-periodic problems to be examined.

The system was released and, during the first 100 iterations, information was gathered on the temperature and normal stress in the X-direction for subsequent use by the temperature and lateral pressure controllers. Equipartitioning occurred within one atomic vibration, (approximately 30 iterations). After 100 iterations, the temperature and pressure controllers were turned on and the system allowed to equilibrate for 900 additional iterations. At 1000 iterations total, the pressure controller was turned off and the system was stored as the equilibrated starting configuration for use in subsequent runs. A picture of this configuration is shown in Figure 8A.

COMPUTATIONAL PLAN

The computational plan involved moving the circle from its central location, shown schematically in Figure 1, towards the upper plate. This motion breaks the symmetry, increasing the distance between the circle and the lower plate. The starting distances from circle to both surfaces of the rectangle were equal to the cutoff radius, $3.87298\,\sigma$. Therefore, the configuration, in effect, represented an isolated particle coming into contact with a free surface of a thin solid. The finite cut-off radius also allowed for relatively small numbers of atoms to represent the planar region since additional atoms outside this cut-off would have only minor effects on the computed behavior.

For argon, the diameter of the circle is 8.6 nm and the height and width of the rectangle are 4.5 nm and 12.9 nm, respectively. It should be noted that the system was periodic in all directions. The effect of a free surface was provided by forming spacings larger than the cut-off radius in the Y- and Z-directions, using a right-handed coordinate system with X to the right and Y directed upward. The Z-direction free surface provided the two dimensionality and the Y-direction spacing allowed the circle to interact with only one surface within the otherwise periodic boundary conditions.

Motion of the circle towards the upper plate was accomplished in three different ways. The first involved controlled displacement. Here, the centroid of the circle and rectangle were computed and, on each successive iteration, the centroid of the circle was reset to position the circle closer to the rectangle. The centroid of the rectangle was reset to the center of the end of the periodic boundary. The velocity of the centroid of both the circle and rectangle were set to zero. This permitted a controlled displacement motion of the circle towards the rectangle. During the motion, however, the individual atoms were allowed to move with the temperature controller running. These adjustments in the atomic positions introduced excess energy to the system. However, the operation of the temperature controller maintained a reasonably ($+1\%$) constant total energy with no long term drift. During the controlled displacement it was noted that the atoms closest to the surface accelerated towards it. This produced a leap-to-contact phenomenon that caused an elastic distortion of the circle.

Once the centroid was at a certain distance (approximately its long term equilibrium position), the motion was halted and the system was allowed to equilibrate without

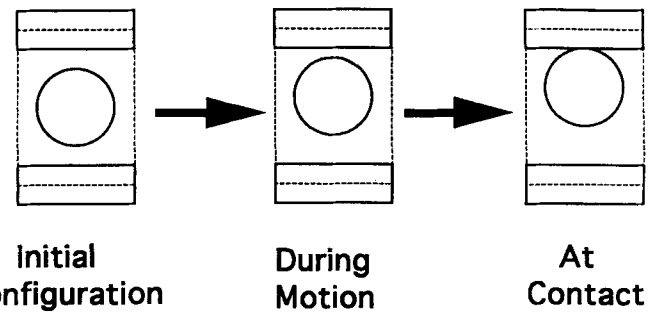

FIGURE 1 Experimental schematic showing circle, rectangle and periodic boundary conditions. The circle is made to move up against the rectangle simulating the approach of a particle to a surface.

further input. The speed of the displacement-controlled motion was 1 cutoff radius in 1000 iterations, each of 0.01 time units. The intentional motion was stopped at a total displacement of 9/10 cutoff radius, or after 900 iterations. This corresponded to a dimensionless velocity of approach of 0.387 σ/t (62.5 m/s for argon). This speed is substantially less than the speed of sound in any medium, and is approximately equal to the speed of a fastball.

The second method also involved a controlled displacement. However, in this instance, the atoms were not allowed to move. This kept the rectangle and the circle in their initial configuration and allowed the forces and potential energies associated with rigid bodies to be calculated.

The last method of approach involved launching the circle towards the upper rectangle with a velocity of 0.387 σ/t. This slow velocity was chosen to avoid complications associated with causing the system to have to dissipate large kinetic energies. The computation was performed with the atoms allowed to move and the circle and rectangle permitted to respond to the forces that developed. It was unnecessary to perfom a "frozen position" computation for the constant initial velocity case because, without atomic motions, the forces and potential energies are a function only of intercentroid distance and the results would be identical to the second case.

Finally, the computational plan included pulling the particle from the surface using displacement control. This was implemented by continuing the first case from the point of initial contact at 1900 total iterations with the sign of the motion reversed. Thus, at the 2800th iteration, the centroid of the circle had returned to its initial position. Although the particle detachment results reported in this paper are only preliminary, they do suggest some interesting effects and are, therefore, included. Further work is in progress to assess the effect of settling and relaxation time on the removal behavior.

COMPUTATIONAL RESULTS

Displacement Controlled Approach

Figure 2 shows the intercentroidal distance, intercentroidal velocity and the apparent surface stress exerted by the circle on the rectangle as a function of the number of iterations. Each iteration represents 0.01 time units. Therefore, at the end of the process, the circle had been in contact with the rectangle for 10,000 iterations of relaxation time, (0.0213 ns for argon). It should be noted that the distance decreased uniformly in time during the approach. The velocity is zero since it is reset by the algorithm after each iteration to avoid any momentum considerations once the system is released. The release of the particle is indicated by the sharp break in the distance *versus* time plot. From the apparent normal stress in the Y-direction, it is seen that the particle experiences initial forces of attraction and repulsion before finally reaching its equilibrium intercentroidal distance. This is a result of the near surface atoms accelerating and hitting the surface, producing wavelike behavior in the system. These waves attenuate with time. The force variations with time due to thermal and acoustic noise are comparable with the initial forces. The stresses may be viewed as the net force on the particle by multiplying by the effective area of 100.017 by 37.4732,

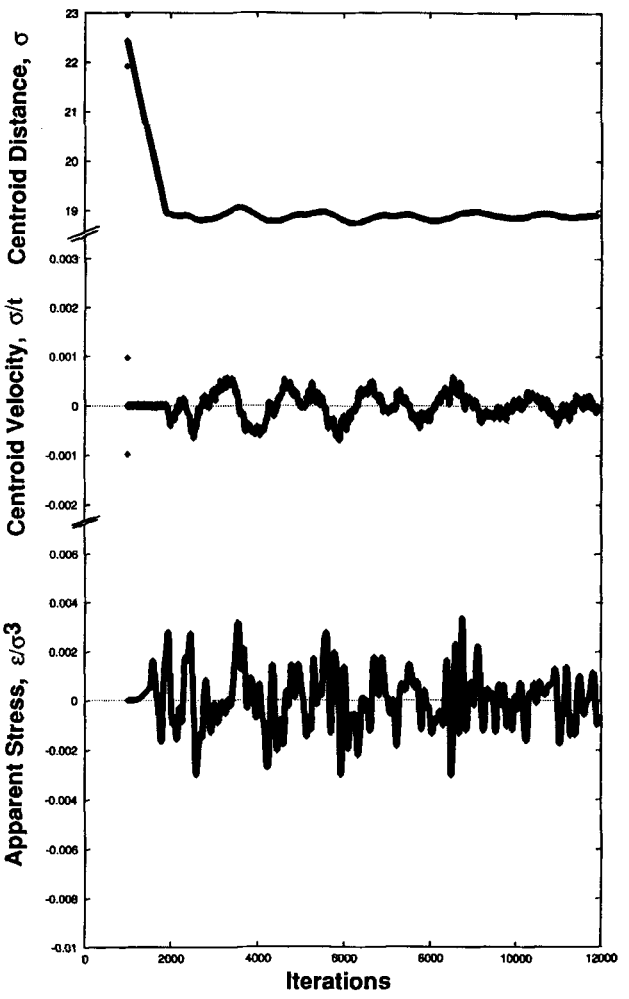

FIGURE 2 Intercentroidal distance, intercentroidal velocity and apparent stress between the circle and the rectangle as a function of time expressed in unit of iterations each of 0.01 dimensionless time units. Fixed displacement control during the approach.

which are the exact dimensions of the periodic boundaries in the Z- and X-directions for these runs.

Fast Pitch

Figure 3 shows the intercentroidal distance, intercentroidal velocity and apparent force on the circle (which equals the stress times fixed area of $3747.96\,\sigma^2$) for the case of the particle thrown at the surface. Some minor fluctuations in the initial velocity due to bending vibrations in the rectangle that developed during equilibration are present. The behavior was dominated by the impact with an accompanying overshoot in the

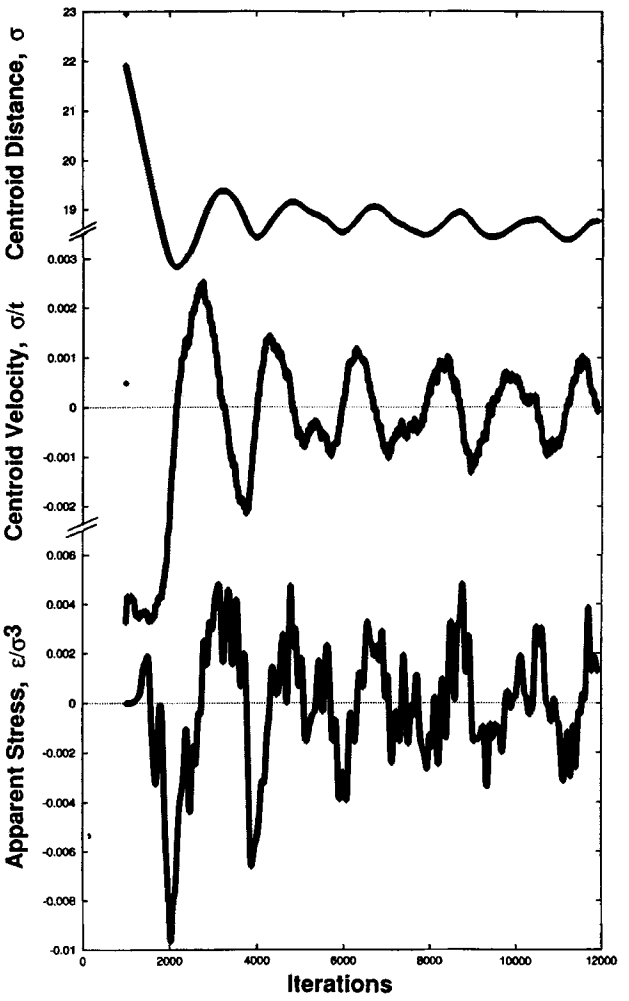

FIGURE 3 Intercentroidal distance, intercentroidal velocity and apparent stress between the circle and the rectangle as a function of time expressed in unit of iterations each of 0.01 dimensionless time units. Free flight during the approach.

initial intercentroidal distances as the rectangle flexed and was indented by the circle. This produced the restoring forces which drove an oscillation. The oscillation appeared to die away exponentially. It should be noted that each graph may be roughly interpreted as the derivative of the one above it. However, minor changes due to thermal and acoustic waves are also present.

In this and the preceding Figure 2, the velocity and displacement information are shown without filtering, whereas the stress information has been smoothed using a 100-point wide Fourier filter.

It can also be seen that the magnitudes of the compressive forces were generally larger than the tensile forces. This is reminiscent of the asymmetry in the potential and

that the distances of closest approach are approximately constant. This is analogous with a ball bouncing lower on each successive bounce. It is of interest to note that the largest tensile stress is less than $0.005\,\varepsilon/\sigma^3$, the value needed to remove the particle in displacement control, as will be discussed in reference to Figure 7.

Distance Velocity Plots: Examining the Dynamics

The dynamics of the controlled displacement and the thrown particle cases, in terms of the distance-velocity plots, are illustrated in Figure 4. The motion of a damped harmonic oscillator on such a plot would appear as a smooth inward spiral to the long term steady state about which the oscillator moves. Examination of the thrown case shows this inward spiral except that it is not symmetric. The asymmetry is a result of the nonlinear character of the force-displacement relationships. The controlled-displacement case appeared to oscillate slightly on this scale. It is important to note, however, that the intercentroidal distances to which these cases are relaxing are not the same. This is a direct result of permanent plastic deformation in the more energetic case, a fact that will become clear once the "pictures" of the configurations are examined.

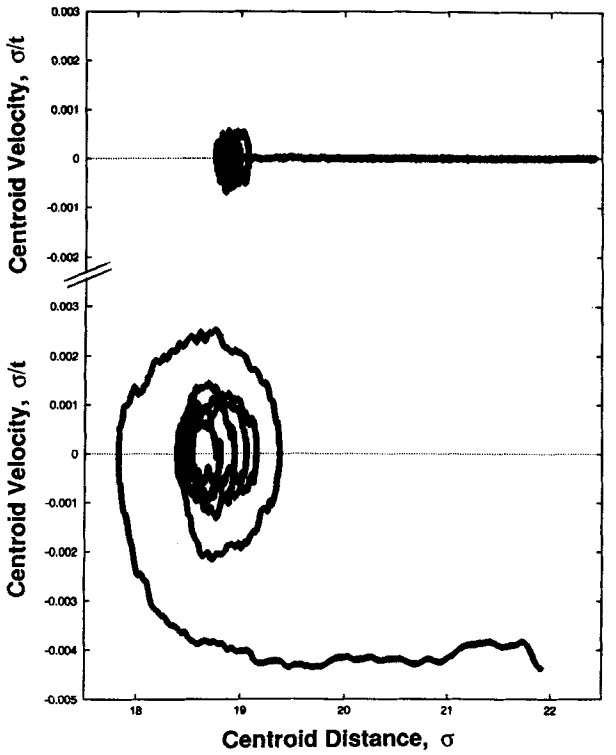

FIGURE 4 Dynamical representation of the decaying oscillations for the two modes of allowing the particle to approach the surface. Note the asymmetric behavior caused by the non-linear potential.

Force Distance Plots: Stiffness Effects

The force *versus* displacement results for the two approach modes are shown in Figure 5. Also shown are the force displacement results associated with the displacement-controlled approach for the case where the positions of the atoms were frozen. When comparing these results, it should be noted that the frozen position case is, essentially, a special case where the bodies interact *via* the interatomic force law but the atoms are constrained. The large forces produced were a result of the leading atoms beginning to overlap the atoms on the surface. This result is unrealistic in that, if such large forces were to be exerted on single atoms, the structure would rearrange as shown in the other two cases. The frozen co-ordinate case, however, is the one associated with a rigid

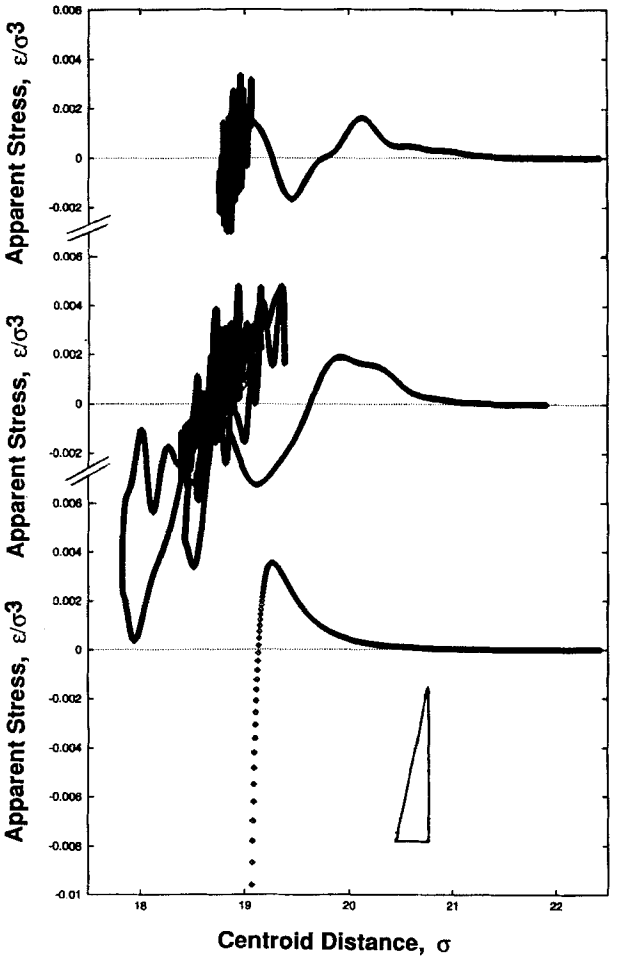

FIGURE 5 Force *versus* displacement curves for the fixed displacement and free flight approach modes compared with the force displacement relation obtained from "freezing" the atomic coordinates to simulate a rigid body.

particle approach used in some of the continuum-based models. Both cases where the atoms can move showed an initial attraction at relatively large separation distances due to the particle and surface deformaions prior to contact. Both also show a repulsion as distance is decreased which gives way to an oscillatory force and displacement about the steady state of zero force at the equilibrium spacing. Again, the particle with an initial velocity has a smaller intercentroidal equilibrium separation than the one in the controlled-displacement case. The repulsion at intermediate distances appears to be a result of the reflection of stress waves. It is not well understood at the present time.

As the oscillations die away, they trace out an inclined line in these graphs. The slope of this line can be interpreted as the apparent elastic stiffness of the particle on the surface. Its value is calculated by multiplying the apparent stress/distance slope by the area. For the case of constant displacement, the slope (in units ε/σ^4) is 0.03. This is multiplied by the area, 3747.96 σ^2, with the resulting stiffness equal to 112.44 ε/σ^2. For the case of argon, the stiffness is found to equal 1.64 N/m. The stiffness of the "thrown" particle is only 1/3 that of the "constant displacement" or 0.55 N/m in terms of the argon parameters. For completeness, a line having a slope corresponding to a reference stiffness of 1.0 N/m is also shown in this figure. It is interesting to note that the calculated stiffness in this study is comparable with that of the cantilevers used in atomic force microscopes.[37] However, the stiffness reported here is for a two-dimensional particle. The stiffness of a three-dimensional particle of comparable radius would be greater because of the larger number of atoms and increased lateral constraints.

Potential Energies

Figure 6 shows the potential energy associated with moving the particle towards the surface with frozen atomic positions. By freezing the atomic positions, thermal noise was eliminated from the computations. This resulted in the very smooth curve shown and facilitates the comparison with other theoretical potentials that might be used to treat this problem analytically. Again, it should be stressed that these calculations are for two-dimensional particle/surface interactions.

Potential energies for the other two cases (not shown) were also examined during the approaches. Oscillations of approximately + 1% of the potential at a frequency corresponding to approximately 450 iterations were observed. These oscillations are apparently due to the flexing of the rectangle, and will be discussed later in this manuscript. The oscillations were either excited by the pressure controller during equilibration or occurred as a natural result of initializing with random Maxwell-Boltzmann distributed velocities. In addition drifts in potential energy of about + 0.25% for the controlled-displacement case resulting from the resetting of the centroidal velocity and position, (*i.e.*, motions not due to the potential, which always add energy to the system) were also observed. Finally, drifts of − 0.25% in potential energy were observed for the thrown case. These were due to the initial action of the temperature controller when the centroidal velocity imparted to the circle caused subtle shifts in the width of the kinetic energy distribution. Because these computations were carried out using the temperature controller, the total energy was controlled and no long term effects accrued.

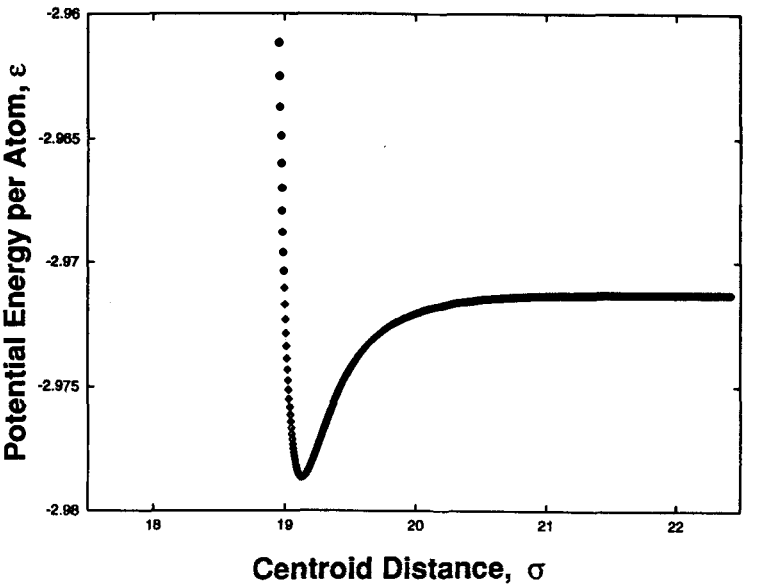

FIGURE 6 Apparent potential energy function for the "frozen" coordinate case. Note that it is essentially a diluted version of the individual interatomic potentials.

Hysteresis on Removal Using Displacement Control: Preliminary Results

As discussed earlier in this paper, adhesion hysteresis is an important factor in understanding a diversity of physical problems including the separation of surfaces and friction. Consequently, it was decided to present early results, obtained from this modeling effort, demonstrating hysteretic effects. More detailed calculations will be presented at a later time.

The apparent stress (force/area), on the ordinate, as a function of intercentroidal distance, on the abscissa, for the displacement-controlled case, is shown in Figure 7. The events corresponding to this case are depicted in Figures 8 and 9. Starting at point *A* in Figure 7, the surfaces were made to approach one another with relatively little interaction until the tensile stress caused the surfaces to leap into contact at point *B*. As the centroids continue to move together, the stress became compressive at point *C*, as expected. Further compression, however, produced an apparent tensile stress as a result of waves propagating throughout the system. Had the system been allowed to equilibrate at points *C* or *D*, a compressive stress would have been observed. Instead, the deformation direction was reversed at point *D*, which produced an oscillating tensile stress. This stress persisted during continuing deformation to point *E*. At point *E* plastic deformation and fracture occurred, with the resulting stresses oscillating about the initial stress level of zero. Thus, this preliminary experiment demonstrated the hysteretic behavior associated with pushing the particle into the surface and immediately removing it without allowing any relaxation time. The data representing the stress was processed by a 100-point wide Fourier filter to smooth the results and partially remove the significant effects of stress waves. The point of displacement direction

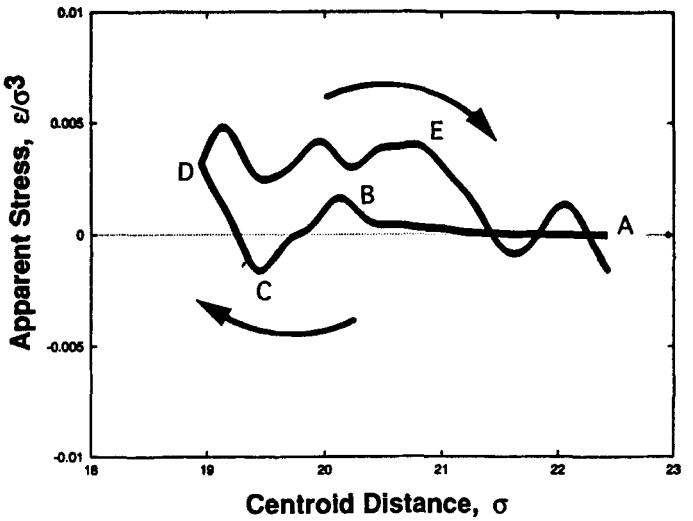

FIGURE 7 Hysteresis behavior as a particle is made to approach and then pulled away from a surface of the same material. The area enclosed by the clockwise look is a measure of the energy dissipated in the process.

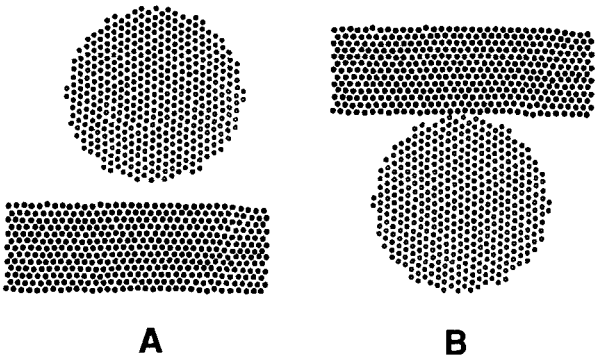

FIGURE 8 (A) Picture of the initial equilibrated system is shown to illustrate the size scale of the cutoff radius. The circle is one cutoff radius from the rectangle. (B) Picture of the circle adjacent to the plate with the coordinates frozen. Note the slight bending of the rectangle.

reversal is indicated by the sharp break in the slope of the curve at minimal intercentroid separation at point *D*.

The maximum apparent stress during removal of the particle from the surface was $0.005\,\varepsilon/\sigma^3$ corresponding to a force of $18.74\,\varepsilon/\sigma$. In terms of argon parameters, this corresponds to 93.9 pN. Once again, these calculations are for a two-dimensional system and would be different (more likely larger) for a true spherical particle. Calculation of the adhesion forces between 8.6 nm particles and a flat plate, assuming that the force can be calculated from the Lifshitz model,[6] with a Hamaker coefficient of

2.0 eV, yields 0.6 nN. Forces associated with the detachment of polystyrene particles from silicon surfaces with the AFM are in the neighborhood of 20 nN[26,27] for attractive interactions between asperity contacts. Considering the approximations employed in this modeling exercise, the results obtained are encouraging and may allow at least qualitative features of adhesion to be examined. Modeling of three-dimensional systems are clearly needed, however, to obtain more quantitative results.

Geometric Representations of the Interactions: A Pictorial Approach

Figures 8–11 show a side view of the circular particle interacting with the rectangular plate. Figure 8A shows the initial configuration after allowing the atoms to equilibrate. The rectangle appears below the circle at a spacing of one cutoff radius, 3.87 σ (corresponding to 1.33 nm for argon). Due to the periodic boundary conditions, the same geometric representation would also occur above the circle. When the circle was raised by 9/10 cutoff radii, it approached the "bottom" of the periodically shifted rectangle as shown in Figure 8B. In this picture, the atoms had been "frozen" in time for the potential and force calculation. This also allowed the "top" and "bottom" of the

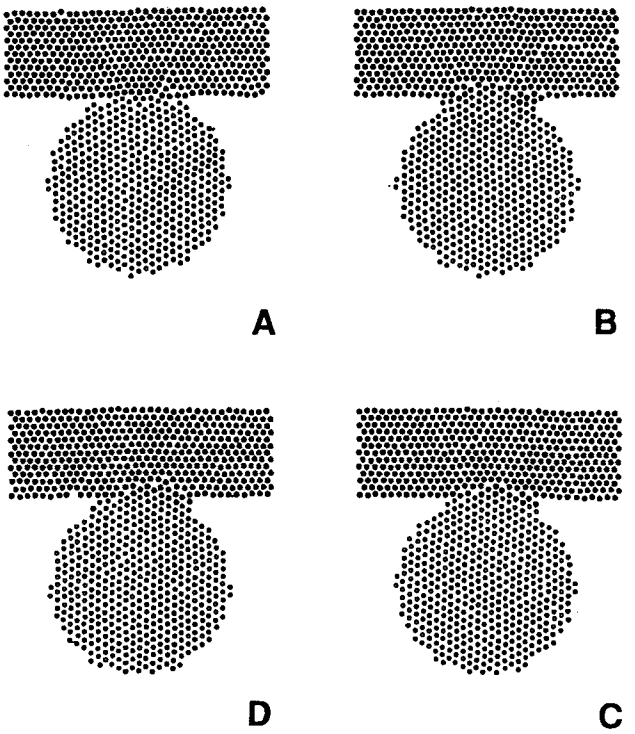

FIGURE 9 Sequence of pictures of the controlled displacement computational results. (A) Shows the particle/surface interaction just after release of the controlled displacement. (B) After a relaxation of 1000 iterations, (C) after a total relaxation of 5000 iterations, and (D) after a total relaxation of 10000 iterations. Detailed changes discussed in text.

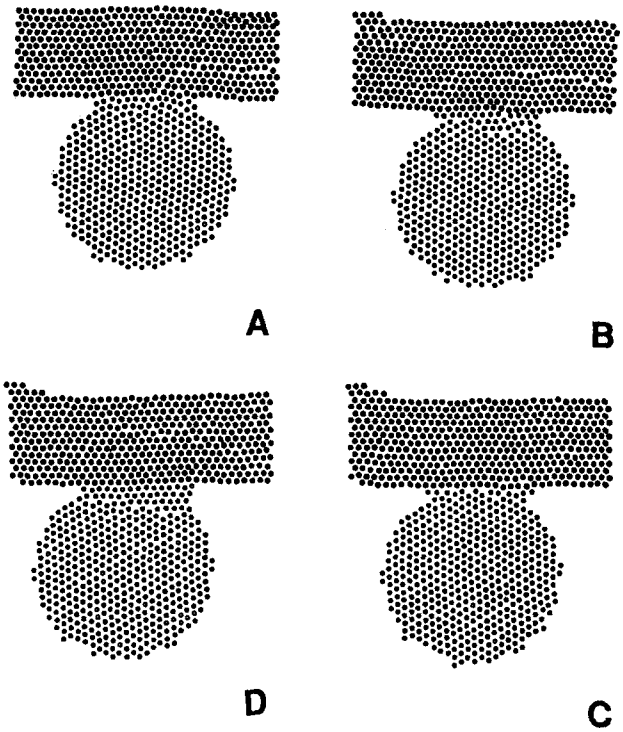

FIGURE 10 Sequence of pictures of the free flight computational results. (A) Shows the particle/surface interaction just impact, (B) after a relaxation of 1000 iterations, (c) after a total relaxation of 5000 iterations, and (D) after a total relaxation of 10000 iterations. Detailed changes discussed in text.

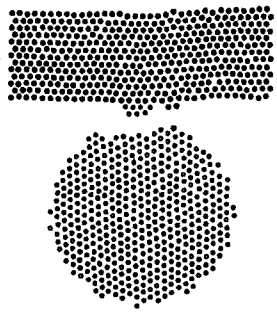

FIGURE 11 Picture showing the geometry of the particle and surface after the particle has been removed from the surface under displacement control. Note that atoms have been transferred both ways and that a dislocation is present in the surface.

circle and rectangle to be identified by features created by their minor asymmetries. An example of such an asymmetry is the slight bending of the rectangle. The rest of the pictures are portrayed with the rectangle drawn above the circle because the circle was moved upward in the computations and did not interact further with the lower

rectangle. Apparent stresses were calculated from the forces between the object and its positively-shifted periodic image. This implies that the apparent normal stresses in the Y-direction are simply the total Y-component of force exerted on the circle by the rectangle divided by the area of the end of the rectangle, 3747.96 σ^2.

Figures 9 shows the sequence of pictures for the displacement-controlled motion case. Figure 9A shows the particle and rectangle at 900 iterations, the point at which the displacement controlled motion was just completed. A dislocation was produced in the rectangle and a fivefold arrangement appeared in the top of the circle, as atoms were displaced from their positions. Figure 9B shows the system after allowing the system to relax for 1000 iterations. The dislocation has disappeared and the circle has resumed its initial geometry on the top edge. Several fivefold arrangements of atoms were in the rectangle which allowed the surface atoms of the rectangle to join coherently with the lattice of the circle. Surface diffusion of the atoms is evident as can be seen by examining the pair of atoms at the five o'clock position with respect to the circle. Figure 9C shows the particle and substrate after the system was allowed to relax for an addition 4,000 iterations (5,000 total). Surface diffusion is again evident, with the atom at the six o'clock position having moved one position. The defect structure in the rectangle has rearranged in a way that appears less coherent with the lattice of the circle. Finally, Figure 9D shows the particle and substrate after the system had been allowed to relax for a total of 10,000 iterations. Surface diffusion, as indicated by the downward motion of the pairs of atoms on both sides of the circle having moved one atom down and the drawing of the atoms from the surface of the rectangle into the meniscus region, is evident on a broad scale. It appears that the surface diffusion is enhanced by the inertia of the material interacting with the propagating elastic waves, as determined in these calculations. Several defects, including fivefold defects, have been formed within the lattice of the rectangle. This allows improved local coherency with the circle. Most of the structural defects appear confined to the rectangle.

When examining these pictures, it is beneficial to compare the physics depicted with the forces, velocities and displacements shown in Figures 2 and 3. For example, Figure 9C is at a total iteration number of 1,900 + 5,000 of relaxation, or 6,900. According to Figure 2 the system should be under local tension at this time. This is consistent with the circle appearing to have moved away from the rectangle at this time.

Pictures of the circle impacting the rectangle after being released at constant (very subsonic) speed are shown in Figure 10. Figure 10A illustrates the centroid having reached its approximate equilibrium position during approach. Again, this corresponds to having traversed 9/10 of the cutoff radius, or 900 iterations, after the initial equilibration time of 1,000 iterations. Thus, the force data for this picture correspond to a total of 1,900 iterations. The smooth bending of the lattice throughout the rectangle due to the stresses associated with the impacting particle is evident in this figure. This may be even more apparent if the diagram is examined from the side. It should also be noted that the deformation of the circle is confined to its first 3 layers of atoms. At this point in time, the back of the circle was still unaware of the impact. There were no dislocations but there was a forced coherency as the circle was "jammed" into the rectangle. Figure 10B shows that slip has occurred in the rectangle after a relaxation time corresponding to an additional 1,000 iterations. For example, a dislocation can be seen in the upper left hand portion of the rectangle. The missing four atoms of its extra

half plane appeared on the top surface of the rectangle. Crack-like open regions also appear within the otherwise perfect crystal inside the rectangle. These defects presumably resulted from propagating stress waves. There is also evidence of the occurrence of surface diffusion in the atoms on the circle at seven o'clock, suggesting that the stress waves from the impact have interacted with the back surface. Additional defects, including fivefold defects in the circle, allowed the coherency with the rectangle to increase.

Figure 10C shows that more surface diffusion has occurred at the seven o'clock position by 5,000 iterations. The defects in the circle have moved towards the interface, thereby reducing the coherency. The dislocation in the rectangle had also slipped out, thereby causing a net rotation of the rectangle. It should be remembered that the rectangle was periodic in the X-direction so that the two planes of slip represent a twist. By 10,000 iterations of relaxation (Fig. 10D), the circle responded to the twist. Having lost symmetry in view of the 30° initial rotational offset, the circle rotated clockwise. Substantial coherency developed as the circle atoms joined the rectangle's lattice. A grain boundary with its associated fivefold defects moved into the circle. By this time, the majority of the lattice defects generated resided in the circle.

Finally, Figure 11 shows preliminary results of returning the centroid of the circle to its initial distance from the centroid of the rectangle. In this example, the particle was literally torn from the surface under displacement control. Atoms of both have transferred, suggestive of cohesive rather than interfacial failure. Surface diffusion occurred, as shown, for example, at the nine o'clock position. A dislocation can be seen in the rectangle corresponding to a missing half plane of three atoms. This dislocation should respond to image forces and slip out if the computation were continued. These preliminary results on particle removal appear very successful at predicting adhesion hysteresis and argue for extending the computations to address the effects of relaxation time on subsequent removal forces.

DISCUSSION

Although the present computations were performed on a two-dimensional lattice, it is clear that many of the features observed are equally applicable to three-dimensional lattices representing spherical particles. In particular, it was observed that the particles and substrates deformed as they approached one another, even in a controlled-displacement mode. This deformation is a manifestation of the leap-to-contact phenomenon often observed in atomic force studies.[25-27] These deformations produce stress waves that propagate throughout the objects. Once the particle and substrate actually contact one another, elastic and plastic deformations can occur in both the particle and the substrate. The structural morphology, that is the detailed arrangement of the atoms, can also change with time. Thus, it is likely that the works of adhesion and removal should be interpreted with this time dependence in mind. The deformations that occur allow the particle and surface to nestle into one another, yet, after relaxation, only a minimum of defects are left behind. Transient defects occurring during the deformation process, such as dislocations, can be created and later disappear but, in the process, provide a means of energy absorption and conversion to heat. It is expected

that these defects can be mobile and re-arrange over time inducing a permanent defect structure. Further computational work is in progress to examine these issues.

Physical values of the parameters can be substituted for the dimensionless units used in this study in order to calculate the actual response of materials to the stresses. For example, if the particle and substrate were argon, the resonant frequency normal to the surface would be 28.7 GHz. The apparent periods of the oscillation shown in Figures 2 and 3 are consistent with this resonant frequency. The accelerations to which the particles are subjected during these oscillations may be calculated by either dividing the force exerted on the particle by its mass or by differentiation of the centroidal velocity *versus* time curves shown in Figures 2 and 3. The results are 3.064×10^{1} m/s^2 and 3.027×10^{12} m/s^2, respectively. Thus, both methods yield an acceleration, for argon, of about 3.11×10^{11} g where g is the acceleration of gravity. As the particles withstand these g forces during vibration, it is clear that such particles cannot be centrifuged off the surface. Although spherical particles would have somewhat different values, the order of magnitude would not be expected to change substantially, thereby making these conclusions qualitatively justifiable for real particles of this size scale. Indeed, qualitatively similar behaviors have been observed using atomic force techniques.[25-27]

Finally, it should be noted that even without effects due to the momentum of the particle, the surface forces in the constant displacement case are sufficiently large to introduce deformations and rearrangements of the atoms in the vicinity of the contact. These surface forces are clearly the dominant influence on such small particles, producing stresses comparable with the theoretical strengths of the materials. Indeed, a very "good" adhesive would be required to keep a 65 m/s bass from bouncing.

SUMMARY

Two-dimensional molecular dynamic computations of particles approaching surfaces have been performed using both displacement control and a fixed initial approach velocity. The displacement, velocity, and force profiles were determined. Graphical "pictures" of the structures were also produced. The computed results form a self-consistent data set that leads to, at least, a qualitative or semi-quantitative understanding of the adhesion of small particles to substrates and the forces and accelerations needed to remove them. Deformations of the particles and surfaces appear to play substantial roles in the adhesion and relaxation processes. Further work in this area should allow the changes in removal forces that develop as the samples are allowed to relax into their steady state configurations to be determined.

Acknowledgements

The authors are grateful to Eastman Kodak Company for support of the computational activity that made this work possible.

References

1. D. S. Rimai, L. P. DeMejo, R. C. Bowen and J. D. Morris, in *Particles on Surfaces 4: Detection, Adhesion, and Removal*, K. L. Mittal, Ed., in press.

2. D. S. Rimai, L. P. DeMejo and R. C. Bowen, *J. Adhesion Sci. Technol.*, in press.
3. R. S. Bradley, *Philos. Mag.*, **13**, 853 (1932).
4. R. S. Bradley, *Trans. Faraday Soc.*, **32**, 1088 (1936).
5. B. V. Derjaguin, *Kolloid Z.*, **69**, 155 (1934).
6. H. Krupp, *Adv. Colloid Interface Sci.*, **1**, 111 (1967).
7. K. L. Johnson, K. Kendall and A. D. Roberts, *Proc. R. Soc. Lond. A*, **324**, 301 (1971).
8. B. V. Derjaguin, V. M. Muller and Yu. P. Toporov, *J. Colloid Interface Sci.*, **53**, 314 (1975).
9. D. Tabor, *J. Colloid Interface Sci.*, **58**, 2 (1977).
10. B. V. Derjaguin, V. M. Muller and Yu. P. Toporov, *J. Colloid Interface Sci.*, **67**, 378 (1978).
11. D. Tabor, *J. Colloid Interface Sci.*, **67**, 380 (1978).
12. V. M. Muller, V. S. Yushchenko and B. V. Derjaguin, *J. Colloid Interface Sci.*, **77**, 91 (1980).
13. V. M. Muller, V. S. Yushchenko and B. V. Derjaguin, *Colloids Surfaces*, **7**, 251 (1983).
14. D. Maugis, *J. Colloid Interface Sci.*, **150**, 243 (1992).
15. D. Maugis, *J. Adhesion Sci. Technol.*, in press.
16. C-J. Tsai, D. Y. H. Pui and B. Y. H. Liu, *Aerosol Sci. Technol.*, **15**, 239 (1991).
17. B. Dahneke, *J. Colloid Interface Sci.*, **40**, 1 (1972).
18. P. Attard and J. L. Parker, *Phys. Rev. A*, **46**, 7959 (1992).
19. J. L. Parker and P. Attard, *J. Phys. Chem.*, **96**, 10398 (1992).
20. D. Maugis and H. M. Pollock, *Acta Metall.*, **32**, 1323 (1984).
21. L. N. Rogers and J. Reed, *J. Phys. D: Appl. Phys.*, **17**, 677 (1984).
22. J. Reed, in *Particles on Surfaces 2: Detection, Adhesion, and Removal*, K. L. Mittal, Ed. (Plenum Press, New York, 1988), pp. 3–18.
23. S. Wall, W. John and S. L. Goren, in *Particles on Surfaces 2: Detection, Adhesion, and Removal*, K. L. Mittal, Ed. (Plenum Press, New York, 1988) pp. 19–34.
24. K. L. Johnson and H. M. Pollock, *J. Adhesion Sci. Technol.*, in press.
25. H. A. Mizes, K.-G. Loh, R. J. D. Miller, S. K. Ahuja and E. F. Grabowski, *Appl. Phys. Lett.*, **59**, 2901 (1991).
26. D. M. Schaefer, M. Carpenter, R. Reifenberger, L. P. DeMejo and D. S. Rimai, *J. Adhesion Sci. Technol.*, **8**, 197 (1994).
27. D. M. Schaefer, M. Carpenter, B. Gady, R. Reifenberger, L. P. DeMejo and D. S. Rimai, *J. Adhesion Sci. Technol.*, in press.
28. L. P. DeMejo, D. S. Rimai, and R. C. Bowen, *J. Adhesion Sci. Technol.*, **5**, 959 (1991).
29. D. S. Rimai, L. P. DeMejo and R. C. Bowen, *J. Appl. Phys.*, **66**, 3574 (1989).
30. D. S. Rimai, L. P. DeMejo, W. B. Vreeland and R. C. Bowen, submitted to *Langmuir*.
31. D. J. Quesnel, D. S. Rimai and L. P. DeMejo, *Solid State Commun.*, **85**, 171 (1993).
32. D. J. Quesnel, D. S. Rimai and L. P. DeMejo, *Phys. Rev. B*, **48**, 6795 (1993).
33. D. J. Quesnel, D. S. Rimai and L. P. DeMejo, submitted to *J. Adhesion Sci. Technol.*
34. J. M. Haile, *Molecular Dynamics Simulations: Elementary Methods* (Wiley, New York, 1992).
35. L. Verlet, *Phys Rev.*, **159**, 98 (1967).
36. J. N. Israelachvili, Y.-L. Chen, and H. Yoshizawa, *J. Adhesion Sci. Technol.*, in press.
37. R. Reifenberger, private communication.